

Cell swelling-induced ATP release is tightly dependent on intracellular calcium elevations

Francis Boudreault and Ryszard Grygorczyk

Research Centre, Centre hospitalier de l'Université de Montréal–Hôtel-Dieu and Department of Medicine, Université de Montréal, Montréal, Québec, Canada

Mechanical stresses release ATP from a variety of cells by a poorly defined mechanism(s). Using custom-designed flow-through chambers, we investigated the kinetics of cell swelling-induced ATP secretion, cell volume and intracellular calcium changes in epithelial A549 and 16HBE14o[−] cells, and NIH/3T3 fibroblasts. Fifty per cent hypotonic shock triggered transient ATP release from cell confluent monolayers, which consistently peaked at around 1 min 45 s for A549 and NIH/3T3, and at 3 min for 16HBE14o[−] cells, then declined to baseline within the next 15 min. Whereas the release time course had a similar pattern for the three cell types, the peak rates differed significantly (294 ± 67 , 70 ± 22 and 17 ± 2.8 pmol min^{−1} (10⁶ cells)^{−1}, for A549, 16HBE14o[−] and NIH/3T3, respectively). The concomitant volume changes of substrate-attached cells were analysed by a 3-dimensional cell shape reconstruction method based on images acquired from two perpendicular directions. The three cell types swelled at a similar rate, reaching maximal expansion in 1 min 45 s, but differed in the duration of the volume plateau and regulatory volume decrease (RVD). These experiments revealed that ATP release does not correlate with either cell volume expansion and the expected activation of stretch-sensitive channels, or with the activation of volume-sensitive, 5-nitro-2-(3-phenylpropylamino) benzoic acid-inhibitable anion channels during RVD. By contrast, ATP release was tightly synchronized, in all three cell types, with cytosolic calcium elevations. Furthermore, loading A549 cells with the calcium chelator BAPTA significantly diminished ATP release (71% inhibition of the peak rate), while the calcium ionophore ionomycin triggered ATP release in the absence of cell swelling. Lowering the temperature to 10°C almost completely abolished A549 cell swelling-induced ATP release (95% inhibition of the peak rate). These results strongly suggest that calcium-dependent exocytosis plays a major role in mechanosensitive ATP release.

(Received 20 July 2004; accepted after revision 4 October 2004; first published online 07 October 2004)

Corresponding author R. Grygorczyk: CHUM–Hôtel-Dieu, 3850 Saint-Urbain, Montréal, Québec, Canada H2W 1T7. Email: ryszard.grygorczyk@umontreal.ca

Adenosine 5'-triphosphate (ATP) regulates diverse biological functions by providing chemical energy for all living cells. As an extracellular mediator, ATP was recognized as the main neurotransmitter in non-adrenergic and non-cholinergic (NANC) postganglionic synapses from efferent autonomic innervation of the gut and bladder (Burnstock *et al.* 1970, 1972). Sensing pain through peripheral afferent innervation, at inflammation sites or from an overloaded bladder, is also thought to be mediated by ATP acting as a neurotransmitter (Birder *et al.* 2003). ATP was found to be costored with acetylcholine in presynaptic vesicles of the neuromotor plate junction (Unsworth & Johnson, 1990) as well as with catecholamines in neuroendocrine chromaffin granules

(Bankston & Guidotti, 1996), supporting its role as a cotransmitter.

Signalling by extracellular ATP is not unique to neurones. Indeed, endothelial as well as epithelial cells release ATP by a regulated non-lytic mechanism (Grygorczyk & Hanrahan, 1997; Bodin & Burnstock, 1998), and express multiple isoforms of ionotropic P2X and metabotropic P2Y receptors (Communi *et al.* 1999; Glass *et al.* 2002). In these cells, ATP release is triggered by mechanical stimuli as diverse as shear stress (Grierson & Meldolesi, 1995), compression (Sauer *et al.* 2000), single cell micropipette stimulation (Stout *et al.* 2002), hypotonic shock (Hazama *et al.* 1999; Niggel *et al.* 2000) and stretch (Grygorczyk & Hanrahan, 1997). Such observations led

to the suggestion that cells respond to mechanical stress by releasing ATP which, in turn, activates the purinergic signalling pathway. It is believed, that such diverse physiological processes as regulation of vascular tone (Burnstock, 1987), airway mucociliary clearance (Morse *et al.* 2001; Chen *et al.* 2001; Lazarowski *et al.* 2004) and lactate secretion from mammary glands (Blaug *et al.* 2003) could involve an autocrine/paracrine loop with ATP serving as an ecto-messenger.

Although vesicular exocytosis is a generally accepted mechanism of ATP release at NANC synapses or from activated blood platelets and chromaffin cells, early studies with other cell types pointed to a channel-mediated process. In epithelial cells, two ATP-binding cassette proteins, the cystic fibrosis transmembrane conductance regulator (Prat *et al.* 1996) and multidrug-resistance proteins (Abraham *et al.* 1993), were implicated in conducting ATP across the cell plasma membrane. Those assertions, however, were contradicted by later studies (Reddy *et al.* 1996; Li *et al.* 1996). Meanwhile, alternative candidates were proposed, such as the hemi-channel connexin (Cotrina *et al.* 1998), the ecto-apyrase CD39 (Bodas *et al.* 2000) and some unidentified stretch-sensitive anionic channels (Mitchell *et al.* 1998; Hazama *et al.* 1999; Sauer *et al.* 2000). The identities of the latter may have been unmasked as voltage-dependent anion channels (VDACs) or VDAC-like channels (Sabirov *et al.* 2001) or volume-sensitive chloride channels (VSCCs) (Hisadome *et al.* 2002).

On the other hand, inhibition of mechanosensitive ATP release by compounds known to interfere with the vesicular trafficking machinery, such as monensin, *N*-ethylmaleimide or the fungal metabolite brefeldin A, indicated involvement of exocytosis (Bodin & Burnstock, 2001; Maroto & Hamill, 2001). Indirect evidence of exocytotic ATP secretion was also demonstrated by the ambiguous pharmacological effects of the trivalent lanthanide gadolinium, which appeared consistent with its action on lipid membrane, rather than direct block of stretch-sensitive channels (Boudreault & Grygorczyk, 2002).

To further investigate the nature of the ATP release pathway, we studied the relationship between the kinetics of hypotonically triggered ATP release, cell swelling and intracellular calcium changes. To cover a wider spectrum of responses, two epithelial cell lines and fibroblasts were tested. ATP release and intracellular calcium changes during hypotonic challenge were evaluated from cell monolayers in a custom-designed flow-through chamber. Hypotonic swelling-induced alterations in the morphology (height, surface and volume) of a single substrate-adherent cell were examined by analysing images recorded in a previously described side-view chamber (Boudreault & Grygorczyk, 2004). Our results show that in response to hypotonic shock, all cells released

ATP in a similar transient manner, despite different kinetics of volume restoration. While the kinetics of ATP release did not correlate directly with cell volume changes, it was strikingly synchronized for all three cell lines with intracellular calcium elevations. Calcium dependence was further demonstrated by the effects of the calcium ionophore ionomycin, which triggered transient ATP release in the absence of cell swelling. In addition, hypotonicity-induced ATP secretion was suppressed by loading cells with the calcium chelator BAPTA, or by lowering the temperature. Our findings are consistent with the concept that calcium-dependent exocytosis is a major mechanism of cell swelling-induced ATP release.

Methods

Cells

Human lung carcinoma A549 cells and murine NIH/3T3 fibroblasts were grown in Dulbecco's modified Eagle's medium supplemented with 10% fetal bovine serum, 20 mM L-glutamine, 60 $\mu\text{g ml}^{-1}$ penicillin-G and 100 $\mu\text{g ml}^{-1}$ streptomycin. Human bronchial epithelial 16HBE14o⁻ cells, a generous gift from Dr D. Gruenert (University of California, San Francisco, CA), were cultured as described (Cozens *et al.* 1994). All constituents of the culture media were from Gibco-BRL (Burlington, ON, Canada). ATP efflux and calcium changes were measured in cell monolayers grown to confluency on 24 mm \times 60 mm glass coverslips. Cellular morphology was analysed in cells plated at low density on 22 mm \times 22 mm glass coverslips.

ATP efflux assay

To measure ATP efflux during hypotonic challenge with high temporal resolution, we used a custom-designed, low-volume (325 μl) flow-through chamber (Fig. 1A). Warm solution (37°C/in-line heater; Warner Instrument Co., Hamden, CT, USA), perfused at a rate of 1.3 ml min⁻¹, was continuously collected for 15 s intervals during the initial burst of ATP secretion (0–10 min), and during 1 or 5 min elsewhere. ATP content in the samples was measured by a luciferase–luciferin-based assay (Boudreault & Grygorczyk, 2002). Because of the finite internal volume of the chamber, washout of ATP released from the cells is a time-dependent process, which distorts the real time course of ATP secretion. To correct for this effect, in a cell-free experiment, we determined the time needed for a 2-fold dilution of a known ATP concentration inside the chamber (Fig. 1B). The chamber was filled with a solution containing 100 nM ATP and then washed. Under these conditions, half-dilution of ATP in the solution was achieved in 15 s. Thus, with a 15 s sampling period, the first sample ($t = 15$ s) at the outlet of the chamber contained only half of the actual amount of ATP released by the cells ($X_0/2$), while the subsequent sample contained

$(X_0/2 + X_1)/2$, etc. With this iterative formula, all ATP efflux data were corrected to eliminate the effect of chamber volume buffering capacity and to measure the exact kinetics of cellular ATP release.

For ATP efflux experiments in the absence of extracellular calcium, calcium-free isotonic saline was perfused for 2 min prior to osmotic shock. According to Fig. 1B, 99% of extracellular calcium was removed from the flow chamber before the onset of osmotic shock. For experiments at low temperature, a custom-made in-line cooler consisting of a small container filled with ice-saturated water allowed reduction of the temperature to 10°C at the inlet of the flow chamber.

Cell volume evaluation

To evaluate cell volume changes of substrate-attached cells, a 3D imaging technique was used (Boudreault & Grygorczyk, 2004). The following is a brief description of the method.

Top- and side-view images. The method involves 3D reconstruction of cell shape based on phase-contrast cell images acquired from two perpendicular directions. Cells grown on a small coverslip were mounted in a custom-designed side-view chamber placed on the stage of a NIKON TE300 inverted microscope (Nikon Canada Inc., Montreal, QC, Canada) and perfused continuously with prewarmed saline (37°C, 1.3 ml min⁻¹). Vertical mounting of the coverslip permitted visualization of the lateral shape of the cell of interest close to the lower edge. After hypotonic challenge, side-view images of the rapidly swelling cell were acquired. In addition, at the beginning and end of an experiment, a top-view image of the same cell was recorded with the coverslip placed in a Petri dish instead.

Imaging. Phase contrast images of the cell's side-view profile and the top-view of the cell base were recorded for 100 ms with a T57 Micromax CCD camera (Princeton Instruments, Trenton, NJ, USA) and MetaFluor software (Universal Imaging, West Chester, PA, USA) at 0.16 µm pixel resolution. Images were saved on hard disk and analysed off-line.

Cell surface reconstruction and visualization. The 3D topography of the cell surface was reconstructed by a dual image surface reconstruction (DISUR) technique, which generates a set of topographical curves of the cell surface from its digitized profile and base outline. Cell volume, surface and height were calculated from such a reconstructed cell topographical model. All calculations were carried out entirely with EXCEL (Microsoft, Redmond, WA, USA). To visualize the reconstructed cell model in 3D perspective, data obtained with the help of the DISUR technique were used to generate a 2D matrix containing approximate z-coordinates of

points on the membrane surface. The 3D perspective of the model cell was then plotted with ORIGIN (Microcal Software, Northampton, MA, USA).

In the course of this study, we observed that a majority of quiescent A549 cells exposed to 50% hypotonic shock remained firmly attached to the substrate throughout the challenge. As a result, the outline of their base remained nearly invariant. Therefore, to reconstruct cell

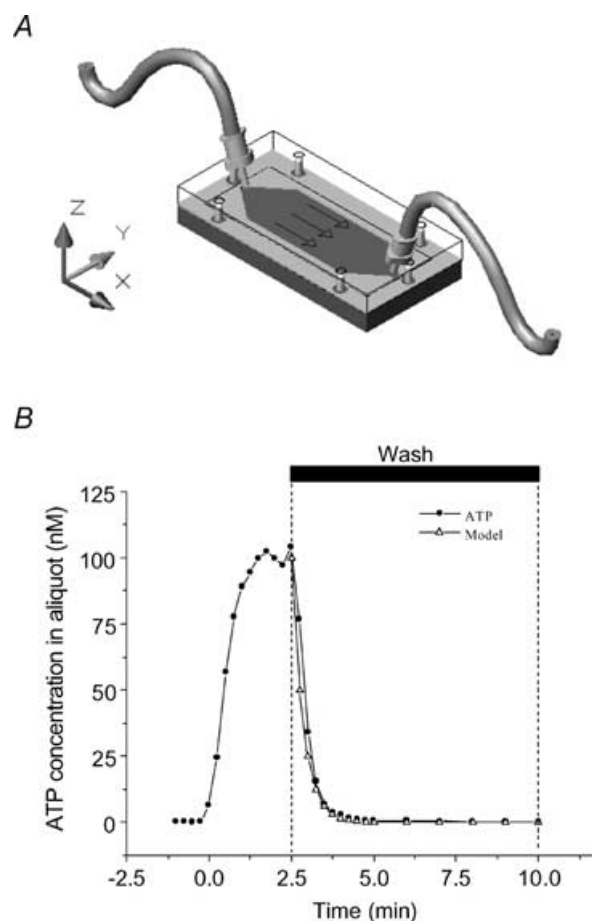


Figure 1. Flow chamber for ATP efflux measurements

A, low-volume flow-through chamber was made of one piece of silicone rubber cut-out from a 0.5 mm thick medical grade sheet tightly pressed between two 6 mm thick polycarbonate plates. The 24 mm × 60 mm glass coverslip with attached cells was inserted between the silicone gasket and the lower plate. The shape of the flow chamber was designed so that laminar flow was achieved throughout 87% of its surface. The surface covered by cells in this laminar section was ~600 mm². At the perfusion rate of 1.3 ml min⁻¹, the maximal theoretical fluid shear generated in the laminar section was 0.16 Pa (1.6 dyn cm⁻²). B, chamber volume buffering capacity was determined in a cell-free experiment. ATP (100 nM) was perfused at the rate of 1.3 ml min⁻¹ through the chamber for 2.5 min then washed away. ATP was evaluated in perfusate samples collected during 15 s intervals. It took 1 min 25 s to wash out 95% of the chamber's ATP content (99% was removed after 2 min). With the configuration used in this study, the time required to dilute the chamber ATP content to half was 15 s. Based on this time constant, the predicted exponential decay describing the dilution is shown in the figure (Δ), which fits very well with the quantity of ATP measured during the wash period (●).

3D morphology at different time points during hypotonic cell swelling, it was sufficient to acquire only a single image of the cell viewed from the top, in addition to a series of side-view images acquired at 15–60 s intervals during the experiment. In contrast, 16HBE14o⁻ and NIH/3T3 cells often demonstrated significant changes in cell base or initiation of migration in response to hypotonic shock. Therefore, only a subset of cells whose base shape remained invariant was selected for 3D reconstruction.

Electrophysiology

For patch-clamp whole-cell experiments, freshly trypsinized A549 cells in suspension were used. Patch pipettes, made from borosilicate glass (World Precision Instruments, Inc., Sarasota, FL, USA), were filled with (mM): 100 CsCl, 90 sorbitol, 2 MgCl₂, 1 EGTA, 1 MgATP and 10 Tes, pH 7.4 (Tris). The bath solution contained physiological saline (see 'Solutions and chemicals'). Whole-cell currents were measured at room temperature with an Axopatch-1C amplifier (Axon instruments, Foster City, CA, USA). Current responses from the computer-generated stimulus waveform were filtered at 2 kHz, digitized (Digidata 1200) at 1 kHz, and recorded on computer by Clampex 8 software. The data were analysed off-line by pCLAMP 8 software. Acute 50% hypotonic shock was achieved by adding appropriate amounts of distilled water to the bath.

Fura-2 calcium measurements

To load Fura-2, cells were incubated (1 h, 37°C, 5% CO₂) in physiological solution containing the acetoxymethyl ester form of Fura-2 (Fura-2-AM, 25 µM; A549 and 16HBE14o⁻) or 50 µM Fura-2-AM + 0.125% pluronic acid (NIH/3T3). For calcium imaging, cells were

mounted in the same flow chamber used for ATP efflux measurements (see Fig. 1A), and perfused with appropriate solutions as described above for ATP efflux assay. To allow microscopy viewing of the cells, the polycarbonate lower plate was replaced by a 0.8 mm thick stainless steel plate having a 13 mm diameter opening in the middle. This permitted through-the-objective illumination of cells for Fura-2 calcium measurements. Changes in calcium were assessed with the microscopy system described above (see 'Cell volume evaluation') which was also equipped for epifluorescent UV illumination. Fura-2-loaded cells were exposed to alternate illumination at 340 and 380 nm with a high-pressure mercury lamp (100 W) via interference filters (Chroma Technology, Brattleboro, VT, USA) mounted on a filter wheel (Sutter Lambda 10-C, Sutter Instrument Co., Novato, CA, USA) and a dichroic mirror (510 nm/540 nm, Chroma Technology). Fluorescence images were recorded during 100 ms exposure at 15–60 s intervals with the digital camera and stored for later analysis. In some experiments, to chelate intracellular Ca²⁺, cells were loaded with BAPTA-AM (25 µM) during 1 h incubation at 37°C and 5% CO₂.

Solutions and chemicals

Physiological saline solution contained (mM): 140 NaCl, 5 KCl, 1 MgCl₂, 1 CaCl₂, 10 glucose and 10 Hepes, pH 7.4, adjusted with NaOH. In Ca²⁺-free saline, CaCl₂ was replaced by 100 µM EGTA. Fifty per cent hypotonic solutions were prepared by reducing salt concentration while keeping divalent cation concentration constant. Stocks of 5-nitro-2-(3-phenylpropylamino) benzoic acid (NPPB), ionomycin and BAPTA-AM were prepared in DMSO at concentrations of 100, 1 and 5 mM, respectively.

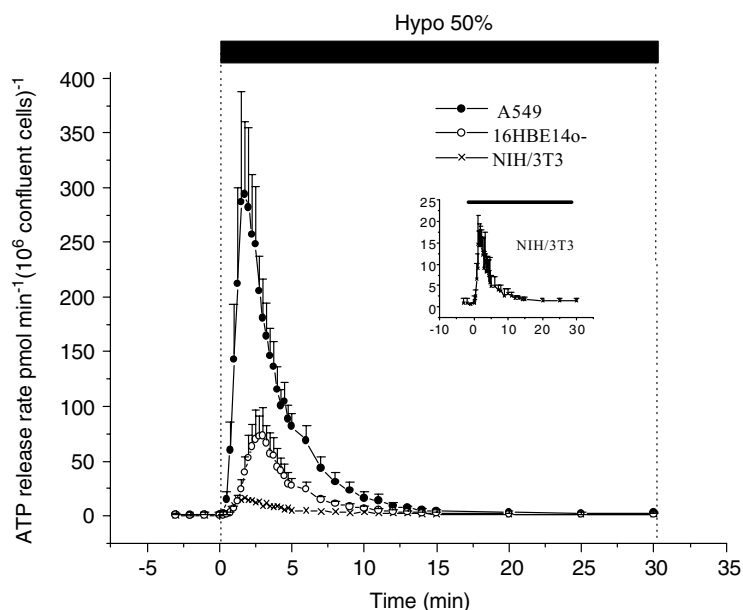


Figure 2. Acute cell swelling induces transient ATP release

ATP secretion from A549, 16HBE14o⁻ and NIH/3T3 cells was markedly enhanced for a short period when fluid tonicity was acutely reduced by 50%. The peak rate of ATP release was many times above its basal level (see Table 1 for details). It was reached in less than 2–3 min, and returned to baseline after 15 min. Inset: ATP secretion from NIH/3T3 cells is shown on an expanded y-axis to show more clearly the transient nature and similarity of ATP release to the other cell types.

Table 1. Basal, peak and cumulative ATP release from hypotonically challenged A549, 16HBE14o⁻ and NIH/3T3 confluent cell monolayers

	Cell density at confluency (cells mm ⁻²)	Basal release (pmol min ⁻¹ (10 ⁶ cells) ⁻¹)	Peak rate (pmol min ⁻¹ (10 ⁶ cells) ⁻¹)	Cumulative ATP released (0–15 min) (pmol (10 ⁶ cells) ⁻¹)
A549 (<i>n</i> = 9)	~500	1.77 ± 0.95	294 ± 67	1002 ± 154
16HBE14o ⁻ (<i>n</i> = 6)	~600	0.87 ± 0.57*	70 ± 22	301 ± 82
NIH/3T3 (<i>n</i> = 6)	~700	0.65 ± 0.75†	17 ± 2.8	78 ± 20

**n* = 5; †*n* = 4.

All reagents were from Sigma (Oakville, ON, Canada) except for Fura-2-AM (Molecular Probes, Eugene, OR, USA).

Results

Kinetics of ATP release

When confluent monolayers of adherent A549, 16HBE14o⁻ and NIH/3T3 cells were subjected to hypotonic swelling, transient ATP release was observed (Fig. 2). The shape of this burst of secretion was very similar for the three cell lines although the amounts of ATP released were quite different. This transient ATP secretion vanished beyond 15 min despite continuous perfusion with hypotonic solution. The data illustrated in Fig. 2 were normalized to 10⁶ cells in a confluent monolayer for two reasons. First, during the course of this study, we observed that the rate of ATP secretion always culminated at 1 min 45 s for A549 and NIH/3T3 cells regardless of cell monolayer density. However, 16HBE14o⁻ cells behaved differently; the timing of peak ATP release shifted from 1 min 45 s to 4 min 45 s when a slightly underconfluent cell monolayer was grown to overconfluency. Furthermore, the peak and total amount of ATP released decreased despite an increasing number of cells in the overconfluent cell monolayer (data not shown). For consistency with the other two cell lines, in this report we only present 16HBE14o⁻ ATP release on the day when they just reached confluency and demonstrated a peak of ATP release at 3 min. The other two cell lines, A549 and NIH/3T3, did not show a decrease of ATP secretion, but a plateau when they reached or exceeded confluency, despite increasing cell density. This suggests, that the amount of ATP released from these cells is mainly proportional to the area covered by cell monolayer and not the number of cells *per se*. The normalized data in Table 1 reveal major differences in terms of total amount of ATP released by different cell types. A549 cells secreted 3 times more ATP than 16HBE14o⁻ and 12 times more than NIH/3T3. Very similar differences were seen for the peak rate of ATP secretion. It is noteworthy that during the experiment, ATP concentration inside the

flow chamber rarely reached 100 nM. At the peak of ATP secretion, its concentration averaged 68 ± 15 nM, 16 ± 5 nM and 3 ± 0.7 nM for A549, 16HBE14o⁻ and NIH/3T3, respectively.

Kinetics of cell volume changes

Figure 3A depicts typical volume changes of substrate-attached cells in response to 50% hypotonic shock. The cells started to swell at a similar rate, which never exceeded 1% s⁻¹. They reached maximal expansion in 1 min 30 s (NIH/3T3) or 1 min 45 s (A549 and 16HBE14o⁻) after onset of the shock. After a plateau which lasted 3 min 30 s for A549 and 5 min for 16HBE14o⁻, the cells underwent a regulatory volume decrease (RVD) while NIH/3T3 remained swollen for 15 min after the shock. We frequently observed for A549 and 16HBE14o⁻ a period of invariant volume (plateau), which preceded RVD. This plateau could only be noted in single-cell volume measurements. It could be overlooked by most other methods, which sum up volume changes from a large cell population. Accordingly, we dissected hypotonic stress-induced volume changes into three different phases: swelling, plateau and RVD. Figure 3A shows that the plateau phase had not been completed by NIH/3T3 cells at 15 min past the shock. Although the duration of volume plateau and RVD varied slightly between individual A549, and especially 16HBE14o⁻, cells (data not presented), maximal swelling was attained during a similar time period for the three cell lines tested.

Since volume changes were evaluated for isolated cells, an important question was whether the same kinetics of volume changes apply to cells that are in close contact with their neighbours in a confluent monolayer. To verify this, we used a lower magnification objective, which allowed us to simultaneously observe, in the side-view chamber, more than a dozen cells in a confluent monolayer. We found that the time course of the 50% hypotonic shock-induced height increase of all cells in the field of view was very similar to that measured for an isolated cell (data not shown). Thus, the volume expansion reported in Fig. 3 for a single cell is likely to represent the typical behaviour of the majority of cells in a confluent monolayer.

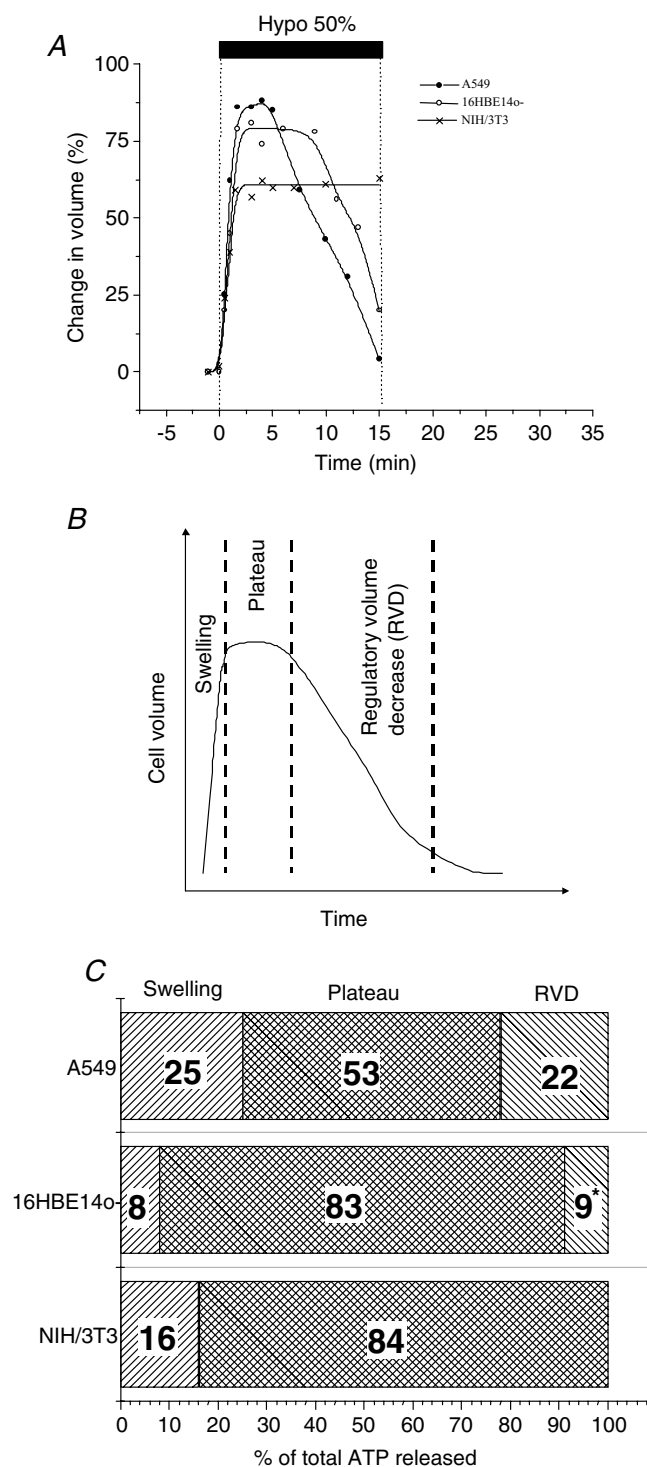


Figure 3. Hypotonic stress-induced volume changes of substrate-adherent cells

A, examples of single A549, 16HBE14o⁻ and NIH/3T3 cell volume changes induced by 50% hypotonic shock (representative of 5 independent experiments for each cell type). Volume changes were evaluated as described in Methods and are expressed as a percentage of the initial volume determined 1 min before the onset of hypotonic shock. Note that cell volume expansion was similar for all three cell types, but significant differences were observed in the time course of volume restoration. B, general pattern of cell volume changes in

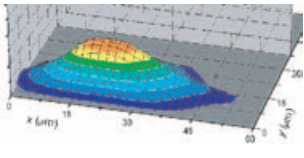
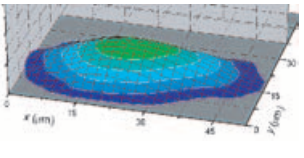
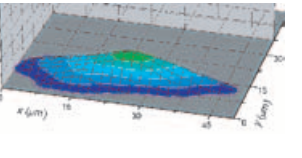
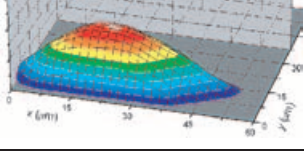
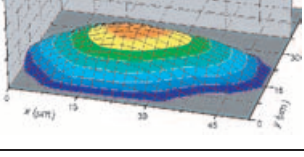
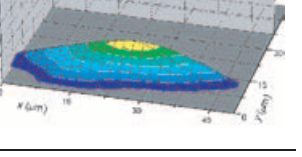
Table 2 presents the morphological parameters: height (*H*), surface (*S*) and volume (*V*) and their changes induced by 50% hypotonic swelling for the three cell types analysed in Fig. 3A. Also, 3D pictures of these cells before and after maximal swelling are shown. It is interesting that volume changes always exceeded 50%, while the cell surface did not grow beyond 12% in those cells. Also, it could be seen that the volume increases were not directly correlated with gains in cell height. For further discussion on swelling-induced cell morphology changes see Boudreault & Grygorczyk (2004).

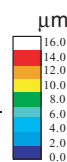
Relationship between ATP release and cell volume changes

Assuming that the majority of cells in a confluent monolayer alter their volume in response to hypotonic challenge in a similar way to the single cell reported in Fig. 3A, one could measure the percentage of ATP secreted during each phase of volume change (Fig. 3B). As illustrated in Fig. 3C, very little ATP (8–25% for 16HBE14o⁻ and A549 cells, respectively) was released during the swelling phase, i.e. when transient rise in membrane tension could be expected. Most animal cells have an excess membrane area beyond that estimated by light microscopy. It buffers membrane tension and allows cells to undergo significant volume and shape changes without rupturing the lipid bilayer. For example, due to large membrane reserves, osmotic swelling or direct inflation of *Xenopus* oocytes did not increase lipid bilayer tension and did not activate stretch-sensitive channels (Zhang & Hamill, 2000). Similar membrane reserves might be expected for A549 cells. Indeed, an adherent A549 cell has a sufficient membrane reservoir to cope even with significant, severalfold volume increases. This is illustrated in Fig. 4, where a cell exposed to extreme (98%) hypotonicity underwent 3-fold volume expansion (200% volume increase) in less than 3 min. The rate of expansion was twice that observed with 50% hypotonic shock. Even larger volume increases (exceeding 400%) were apparent for some cells (data not shown). Thus, at maximal volume increase induced by 50% hypotonic shock, the cells are far from depleting their membrane reserves. One may expect that in such cells, due to the combined effects of excess membrane and its viscoelastic properties, bilayer tension could only rise transiently during dynamic volume increase and should vanish during quasi-static conditions

response to 50% hypotonic shock, which includes three distinct phases: swelling, plateau (invariant volume) and regulatory volume decrease (RVD). C, the cumulative amount of ATP released during each period described in B was calculated from Fig. 2 and expressed as a percentage of total ATP released during 15 min post shock. Note that very little ATP was released during cell swelling. * ATP efflux terminated before completion of RVD.

Table 2. Morphological parameters (height, H ; surface, S ; volume, V) of A549, 16HBE14o $^-$ and NIH/3T3 cells before hypotonic shock and when reaching maximal volume expansion

	A549			16HBE14o $^-$			NIH/3T3		
	H (μm)	S (μm^2)	V (pl)	H (μm)	S (μm^2)	V (pl)	H (μm)	S (μm^2)	V (pl)
Time 0	13.5	2914	5.2	9.4	2793	4.0	9.6	1316	1.5
									
Maximal expansion ($t = 1 \text{ min } 30 \text{ s}$ or $t = 1 \text{ min } 45 \text{ s}$)	16.0	3249	9.7	12.8	3015	7.2	11.7	1471	2.3
									
% increase	H 19	S 11	V 86	H 36	S 8	V 78	H 22	S 12	V 53



at volume plateau. We found in this study that most ATP is secreted during volume plateau and only a small fraction during the swelling phase. This demonstrates that most ATP is released via mechanisms other than stretch-activated channels (Taylor *et al.* 1998) or exocytosis of vesicles whose trafficking or fusion is facilitated by heightened membrane tension.

Role of volume-sensitive chloride channels (VSCCs) in ATP release

From Fig. 3C it is apparent that only a small fraction of ATP was released during volume restoration. Since this is a period where one might expect maximal activity of VSCCs, it indicates that such channels are unlikely to play a major role in ATP secretion. Many previous studies, however, reported inhibition of ATP release by NPPB, which is a potent blocker of various chloride channels, including VSCCs. These findings suggested a potential role of NPPB-inhibitable channels in ATP release. We investigated this in A549 cells, which could secrete as much as 22% of ATP during volume restoration, (Fig. 3C).

Whole-cell patch-clamp experiments demonstrated the presence of VSCCs in A549 cells, which were almost completely blocked by 125 μM NPPB (95% inhibition; Fig. 5A). Cell swelling-induced whole-cell currents showed characteristic outward rectification and inactivation at large depolarizing membrane potentials (Fig. 5B and C, respectively). Figure 6 illustrates the effect of NPPB

on hypotonicity-induced cell volume changes and ATP release. In these experiments, to minimize the non-specific effects of NPPB on cell physiology (see below), it was only applied during hypotonic shock. Because VSCC currents are almost completely abolished by NPPB in less than 1 min (Fig. 5A), a near-complete block was expected before the onset of RVD. In the presence of 125 μM NPPB in the bath, cells swelled at a rate similar to that under control conditions (Fig. 3A). However, RVD, which normally starts 5 min after hypotonic shock (Fig. 3A), was completely abolished, and cells remained maximally swollen for the next 18 min. At 20 min, the NPPB block was removed by washing away the drug. This resulted in immediate cell volume restoration. Interestingly, despite relieving the VSCC block, no parallel increase of ATP release was observed, demonstrating that ATP does not permeate via VSCCs. Nevertheless, significant inhibition of ATP release (81% inhibition of peak and 73% inhibition of cumulative) was observed in the presence of NPPB (compare Figs 6 and 2). In a separate experiment in a test tube we noticed that NPPB diminished light output from the chemiluminescent luciferase–luciferin reaction, with $\text{IC}_{50} = 525 \mu\text{M}$ (Fig. 7). It should not, however, interfere with our ATP efflux measurements, since the concentration used in this study did not exceed the threshold of inhibition, $\sim 250 \mu\text{M}$ (Fig. 7). The ability of NPPB to strongly block a bioluminescent reaction raises concern about the specificity of this chloride channel blocker, as already reported (Brown & Dudley, 1996; Kato *et al.* 1999).

Kinetics of intracellular calcium changes

Ratiometric Fura-2 fluorescence experiments revealed that hypotonic challenge of the A549 cell monolayer raised $[Ca^{2+}]_i$ in the majority of cells. Individual cells, however, responded in many different ways, some experiencing a single, or multiple, spike(s), others monotonical increases of $[Ca^{2+}]_i$ (Fig. 8). When the responses from a large number of cells were averaged (approximately 600 cells), a transient $[Ca^{2+}]_i$ increment was observed that reached a peak 1 min 45 s after the shock and was followed by a decline to a slightly elevated level (Fig. 8, bold trace). Interestingly, this averaged signal demonstrated a strong similarity to the ATP release curves in Fig. 2. To highlight the synchronicity seen between changes in $[Ca^{2+}]_i$ and ATP release for A549 cells, both traces were plotted in Fig. 9 (left panel). A simultaneous rise of both signals, $[Ca^{2+}]_i$ and ATP release, was also discerned for 16HBE14o⁻ and NIH/3T3 cells (Fig. 9, middle and right panels). Such synchronicity is not only a demonstration of the calcium dependence of swelling-induced ATP release but also that the mechanism of ATP release might be archetypal, since all three cell lines presented a very similar profile of ATP release and $[Ca^{2+}]_i$ changes. In addition, when 16HBE14o⁻ cell monolayers were grown below confluency, the hypotonicity-induced peak of $[Ca^{2+}]_i$

occurred approximately 1 min sooner. Interestingly, this was also accompanied by a similar 1 min earlier appearance of the peak rate of ATP release (data not shown). These results strongly suggest a close association between the rate of ATP release and $[Ca^{2+}]_i$ elevations. Both $[Ca^{2+}]_i$ and ATP signals in Fig. 9 are averaged from a large number of cells. If this tight relationship holds true for each individual cell, it may indicate that ATP could be released in a slightly different fashion from each cell, reflecting variable $[Ca^{2+}]_i$ responses of individual cells within a monolayer (see Fig. 8).

To further investigate the role of $[Ca^{2+}]_i$ in ATP release, we tested the ionophore ionomycin, which has been widely used as a non-specific secretagogue for many cell lines (Unsworth & Johnson, 1990). Exposure to 5 μ M ionomycin for 3 min induced transient ATP release from A549 cells. This release reached 18% of the peak rate, and 12% of the total amount of ATP, when compared to release induced by 50% hypotonic challenge (Fig. 10A, bottom trace). The peak of this transient release was reached in less than 1 min 30 s, similar to the time required for a maximal increase in $[Ca^{2+}]_i$ (Fig. 10A, upper trace). In addition, significant inhibition of swelling-induced ATP release (71% inhibition of peak and 63% inhibition of cumulative release) was observed for A549 cells loaded with the Ca^{2+} chelator BAPTA (Fig. 10B). These experiments strengthen the notion that hypotonic stress-induced ATP release requires elevation of $[Ca^{2+}]_i$. For A549 cells, this $[Ca^{2+}]_i$ elevation appears to originate almost exclusively from intracellular stores. In preliminary experiments, we did not detect any diminution of ATP release induced by 50% hypotonicity in calcium-free solution ($n = 3$, data not shown). This also demonstrates that in our study putative Ca^{2+} influx via plasma membrane stretch-sensitive channels is not involved in ATP secretion. Our results are consistent with the previously reported observation that intracellular calcium stores are the main source of hypotonically induced calcium elevation in embryonic rat aorta cells (Missiaen *et al.* 1996).

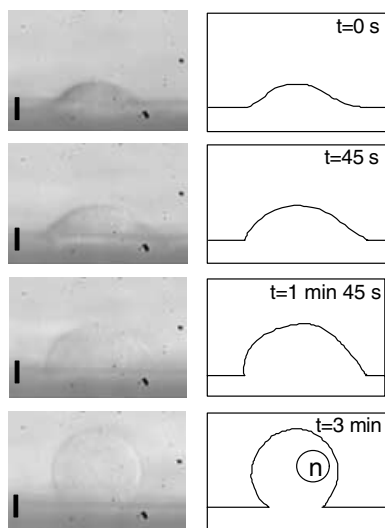


Figure 4. A549 cells have a large membrane reservoir

Substrate-adherent A549 cells were mounted in the side-viewing chamber and exposed to 98% hypotonic solution. A sequence of images (left panels) shows changes of a cell side profile recorded during swelling at the indicated time points. For clarity, corresponding outlines of the cell profile were also drawn (right panels). The estimated volume increases were approximately 80% at 45 s, 150% at 1 min 45 s, and > 200% at 3 min. In the vast majority of cells, volume increased more than 200% (3-fold), and in some cases went beyond 400% (at 5–10 min, data not shown) before cell rupture. The solution contained 1 mM $MgCl_2$ and 1 mM $CaCl_2$ (~98% hypotonic). The scale bar corresponds to 10 μ m and 'n' represents the nucleus.

ATP release and $[Ca^{2+}]_i$ elevations are abolished at low temperatures

A strong calcium dependence of ATP release suggests the involvement of vesicular exocytosis, a mechanism that could be significantly inhibited by lowering the temperature. Consistent with this notion, when A549 cells were cooled to 10°C, swelling-induced ATP release was almost completely suppressed, with 95% inhibition of the peak rate and 85% diminution of ATP accumulation (Fig. 11A). It is remarkable, that at this temperature, the $[Ca^{2+}]_i$ increase induced by 50% hypotonic shock was also completely abolished (Fig. 11B). Interestingly, cells swell to the same extent as at 37°C, albeit at a slower pace (data

not shown). This inhibition could not be explained by temperature effects on Fura-2, because in the absence of hypotonic shock, the basal fluorescence ratio remained unchanged during cooling. This agrees with a previous report that ratiometric calcium measurements with freshly prepared Fura-2 are not affected by temperature changes in the range of 5°–40°C (Oliver *et al.* 2000).

Discussion

In the present study we measured the kinetics of cell swelling-induced ATP release, cell volume and intracellular Ca^{2+} changes of substrate-adherent cells with sufficiently high temporal resolution to analyse the relationship between the three processes. This allowed us to evaluate the potential contribution of specific ATP release mechanisms. Among many putative ATP release mechanisms, two may be triggered solely during cell expansion, when membrane tension is expected to rise transiently. One may involve ATP-conducting channels directly activated by membrane stretch. The second may occur via exocytosis of ATP-filled vesicles, whose fusion with the plasma membrane is favoured by increased membrane tension during cell swelling. Another mechanism assumes that ATP conduction through a broad family of VSCCs may contribute to ATP secretion, mainly during cell volume restoration. Finally, conductive ATP release may proceed through VDAC-like channels or connexin hemichannels, but no specific time frame could be assigned, since the mechanism of their

activation is not well characterized. For the purpose of this discussion, we assume that these channels may be active at any time after hypotonicity-induced cell swelling.

The first two mechanisms fail to properly describe the ATP release kinetics observed in the present study, since only a small fraction of ATP (8–25%) is released during the swelling phase. Furthermore, our previous experiments with Gd^{3+} , a blocker of mechanosensitive channels, also did not support the view that such channels are involved in ATP release (Boudreault & Grygorczyk, 2002). These two mechanisms therefore could be excluded as major players in the cell swelling-induced ATP secretion seen in our study. It is also unlikely that VSCCs mediate ATP release, although some ATP is released (especially by A549 cells, up to ~22%) during VSCC-mediated RVD. Indeed, when A549 cells were swollen in the presence of NPPB, washout of the drug to relieve block of VSCCs did not result in ATP secretion despite the fact that the channels were functional, as demonstrated by a rapid cell volume decrease (Fig. 6). Failure of VSCCs to conduct ATP is consistent with an earlier report by Hazama *et al.* (1999). Although ATP release was diminished by NPPB, it could not be interpreted as an indication of VSCC involvement because of broad effects of the compound. The exact cause of this inhibition remains to be investigated. The last category, maxi-anion or VDAC-like channels, remains a possible pathway for conductive ATP release, although it is difficult to accept that during ATP secretion from swollen cells, such large anion conductance did not induce

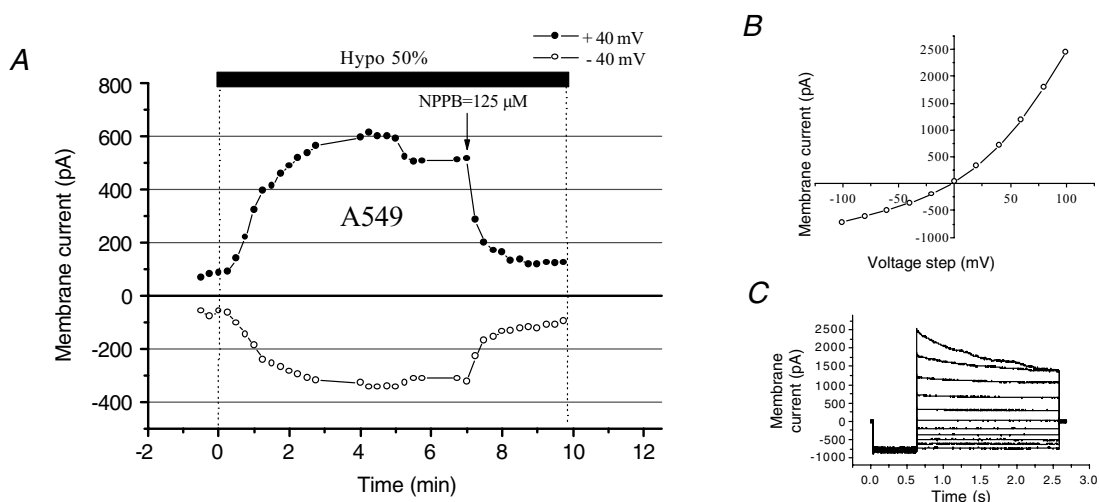


Figure 5. Cell swelling-induced whole-cell current in A549 cells

A, representative whole-cell currents recorded every 15 s in response to alternate 100 ms pulses from 0 to ± 40 mV. Hypotonic shock (50%) was applied by diluting the bath medium with distilled water. This resulted in a rise of whole-cell current, which was rapidly blocked by the bath addition of NPPB (arrow). B, the current–voltage relationship measured at the beginning of the pulses, shown in C, displays typical outward rectification as expected for volume-sensitive current. C, current traces in response to 2 s voltage steps from -120 to $+120$ mV in 20 mV increments. The holding potential was 0 mV, and prepulse, -120 mV. Note the small inactivation at high depolarizing voltages.

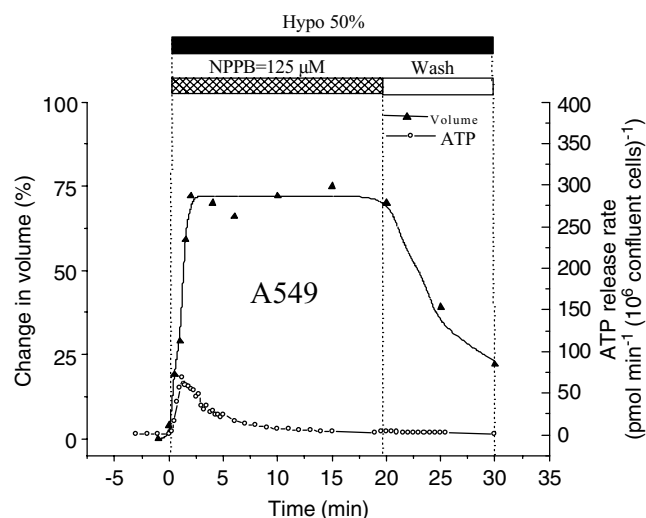


Figure 6. Effects of NPPB on cell volume and ATP release

This figure combines the results from 2 separate experiments. The upper curve (\blacktriangle) shows hypotonic stress-induced volume changes of a single A549 cell observed in the presence of NPPB, and after washout of the drug. The trace seen here is representative of 3 experiments. Volume changes are expressed as percentage of initial volume (at $t = -1$ min). The lower curve (\circ) indicates the rate of ATP release from a monolayer of A549 cells in the presence of NPPB and after its wash (representative of 3 experiments). Note that washing away NPPB initiated the volume restoration process, but it was not paralleled by an increase of ATP release.

a concomitant cell volume decrease. If ATP liberation proceeds via activated high-conductance anion channels, smaller osmolytes, such as Cl^- , should also escape the cell and contribute to RVD. Figure 3C contradicts such

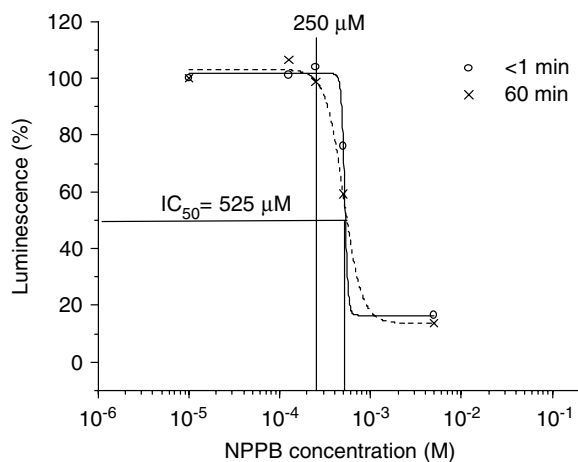


Figure 7. Effect of NPPB on luciferin-luciferase luminescence

ATP (final concentration 100 nM) was added to a 50% hypotonic cell-free solution containing increasing concentrations of NPPB (10 μM to 5 mM). ATP-dependent luminescence was evaluated immediately, or 1 h later, by a luciferase-luciferin-based assay, and is shown as percentage of maximal luminescence. NPPB dose-dependently inhibited luminescence, although the effect was time independent. No inhibition was apparent below 250 μM NPPB. Data are the means of 3 independent experiments.

expectations and demonstrates that all three cell lines tested in our study secreted ATP mainly during volume plateau (53–84% of total released ATP), i.e. in the absence of noticeable cell volume changes. Thus, in our view, none of the above mechanisms could satisfactorily explain the nature and kinetics of cell swelling-induced ATP release.

Our experiments provide strong evidence for the involvement of intracellular Ca^{2+} in ATP release. This includes the following: (i) the time course of ATP release is strikingly coordinated with intracellular Ca^{2+} elevations; (ii) ATP secretion could be evoked solely by a rise in intracellular Ca^{2+} , i.e. in the absence of hypotonic cell swelling; (iii) ATP release is significantly inhibited by chelating intracellular Ca^{2+} . Such tight Ca^{2+} dependence is expected from an exocytotic release mechanism, and this notion is further supported by a strong inhibitory effect (95% peak inhibition) of low temperature. The extent of such inhibition by low temperature or Ca^{2+} chelation suggests that Ca^{2+} -dependent vesicular exocytosis is the main mechanism of cell swelling-induced ATP release and the contribution of other mechanisms is negligible. Low temperature is often used to inhibit exocytosis, which involves many highly temperature-sensitive steps, such as vesicle trafficking or membrane fusion. In this study, we found complete inhibition of $[\text{Ca}^{2+}]_i$ elevation at 10°C despite near-normal cell swelling. While, this effect needs further investigation, it could alone cause full inhibition

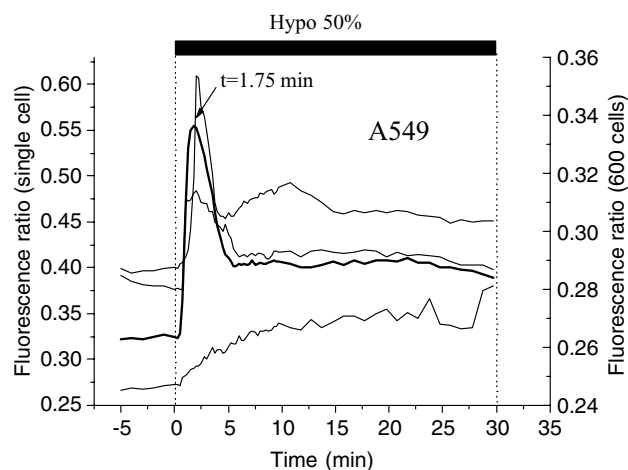


Figure 8. Intracellular calcium changes in response to 50% hypotonic challenge

Coverslips with Fura-2-loaded A549 cells were mounted in a modified version of the flow chamber (see Methods). Fluorescence images were recorded every 15 s during the course of 50% hypotonic challenge. Cytosolic calcium responses are shown from 3 individual cells (thin lines) in a field of view (FOV) localized in the centre of the flow chamber. It reveals variability of the response among individual cells, but when the responses were averaged for the entire FOV, a single calcium spike at 1 min 45 s was observed (thick line). There were approximately 600 cells in the FOV (0.2% of the total number of cells covering the coverslip).

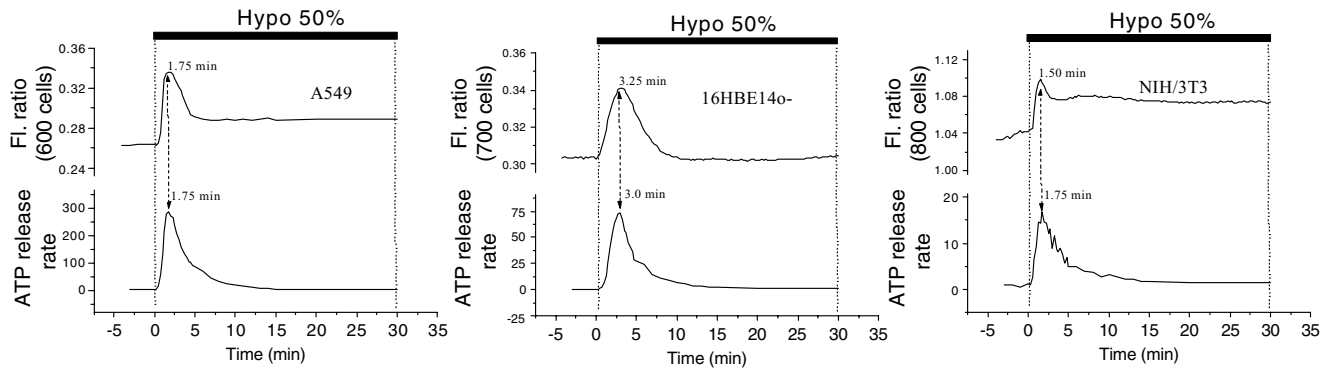


Figure 9. Hypotonic stress-induced ATP release is synchronized with $[Ca^{2+}]_i$ changes

Peak ATP release occurred almost simultaneously with cytosolic Ca^{2+} elevations for all 3 cell lines, and the corresponding peak times are indicated on the figure. The differences did not exceed the temporal resolution of these measurements (~ 15 s). Graphs showing the ATP release time course from A549, 16HBE14o⁻ and NIH/3T3 cells (lower traces; units are pmol min^{-1} (10^6 confluent cells)⁻¹) are reproduced from Fig. 2. Changes of $[Ca^{2+}]_i$ (upper traces, fluorescence ratio (FI. ratio)) were measured in a separate experiment, as described in Fig. 8, and are representative of 3 experiments for each cell line.

of exocytosis. It should also be noted that the strong effect of low temperature cannot exclude the contribution of other pathways, such as a highly temperature-sensitive ATP transporter. However, several characteristics of ATP release, such as the kinetics or Ca^{2+} dependence make such a hypothesis very unlikely. Although it has been suggested recently that fusion of vesicles could deliver ATP-conductive channels to the plasma membrane (Gatof *et al.* 2004), we favour non-conductive direct secretion

of ATP stored in vesicles. We base our reasoning on two factors. First, as discussed above, cell volume remains invariant during a period when a large amount of ATP is released, indicating a non-conductive mechanism. Second, ATP had been found to be stored in secretory vesicles from a large number of cell types. Although the identity of vesicles responsible for storage and mechanosensitive ATP secretion from epithelial cells remains to be identified, it could belong to the same family of ATP-laden vesicles that

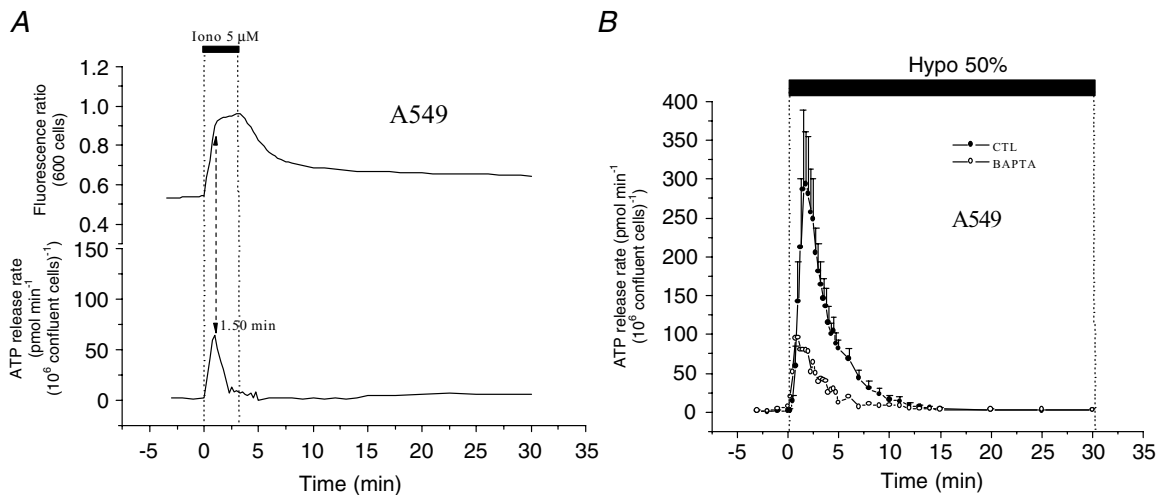


Figure 10. Modulation of ATP release by intracellular calcium

A, in the absence of hypotonic shock, application of $5 \mu\text{M}$ ionomycin (Iono) to A549 cells resulted in a robust $[Ca^{2+}]_i$ increase within 1.5 min (upper trace). In a separate experiment, ionomycin triggered transient ATP release (lower trace), which peaked at 1.5 min and vanished in less than 5 min. In this example, the peak rate of ATP secretion reached 53 pmol min^{-1} (10^6 confluent cells)⁻¹, and the total amount of released ATP was 120 pmol (10^6 confluent cells)⁻¹ (representative of 3 independent experiments). Note the similarity in the rise of $[Ca^{2+}]_i$ and ATP secretion. **B**, loading A549 cells with the Ca^{2+} chelator BAPTA diminished hypotonic stress-induced ATP release (○). The peak rate of ATP secretion was 85 pmol min^{-1} (10^6 confluent cells)⁻¹, while the cumulative ATP release was 370 pmol (10^6 confluent cells)⁻¹. The trace showing ATP secretion from untreated cells (CTL, ●) is reproduced from Fig. 2.

had been previously reported in non-neuronal cells, such as adrenal or pancreatic cells (Bankston & Guidotti, 1996; Hazama *et al.* 1998).

An exocytotic mechanism of ATP release could also explain the previously reported release of other nucleotides, such as uridine triphosphate (UTP), which is released in a similar fashion to ATP by fluid flow-induced mechanical stress (Lazarowski *et al.* 1997). It is reasonable to postulate that they originate from the same pool of vesicles since ATP and UTP are both substrates of the chromaffin granule nucleotide transporter (Bankston & Guidotti, 1996), a transmembrane transport protein also likely to be found on ATP-filled organelles.

It might be interesting to analyse previous studies that used a similar experimental protocol of Ca^{2+} ionophore and/or BAPTA-AM, but did not detect direct stimulation or inhibition of ATP release (Grygorczyk & Hanrahan, 1997; Maroto & Hamill, 2001). In our previous investigations we did not observe the stimulation of ATP release by Ca^{2+} -mobilizing agents (A23187, histamine or carbachol) in human lung adenocarcinoma (Calu-3) cells (Grygorczyk & Hanrahan, 1997). This might be attributed to the very transient nature of such release (see Fig. 10), lower sensitivity and poor temporal resolution of the ATP efflux/accumulation assay in that study compared to the flow chamber approach in experiments described in the present report. These problems may be even more profound in oocytes where, in the absence of vigorous mixing, ATP diffusion could be significantly limited, especially by the oocyte vitelline layer, contributing to the formation of an

unstirred layer at the oocyte membrane. Indeed, Maroto & Hamill (2001) found no effect of A23187 on basal ATP release but noticed 10-fold potentiation of release stimulated by medium puffing, which was attributed to facilitation of vesicle fusion during intra-Golgi transport. Furthermore, BAPTA loading did not prevent mechanosensitive ATP release from oocytes, which contrasts with our results on A549 cells (Fig. 10B). In addition, we did not observe the potentiation of ATP release when ionomycin and hypotonic stimuli were applied together. In such experiments, the peak of ATP release remained almost unchanged, but occurred ~ 30 s earlier compared to the release induced by hypotonic shock alone (data not shown). This strengthens the notion that intracellular Ca^{2+} elevation is a critical step in ATP release.

Additional interesting observations that emanate from the analysis of our data are related to cell volume. Previous studies reported volume changes in response to 50% hypotonic shock, ranging from 10 to 39%, when measured by various methods with different substrate-attached cell types (Bibby & McCulloch, 1994; Raat *et al.* 1996). However, Coulter-counter analysis of the same cells revealed much higher volume increases, up to 70–74% (Bibby & McCulloch, 1994; Raat *et al.* 1996), similar to that observed with red blood cells (Light *et al.* 1999) and close to those in the present study with substrate-adherent cells (53–86%). It could be speculated that other methods which indirectly evaluate the cell volume of substrate-adherent cells, e.g. by measuring only cell height or fluorescence intensity of fluorophore-loaded cells, may underestimate the actual volume changes.

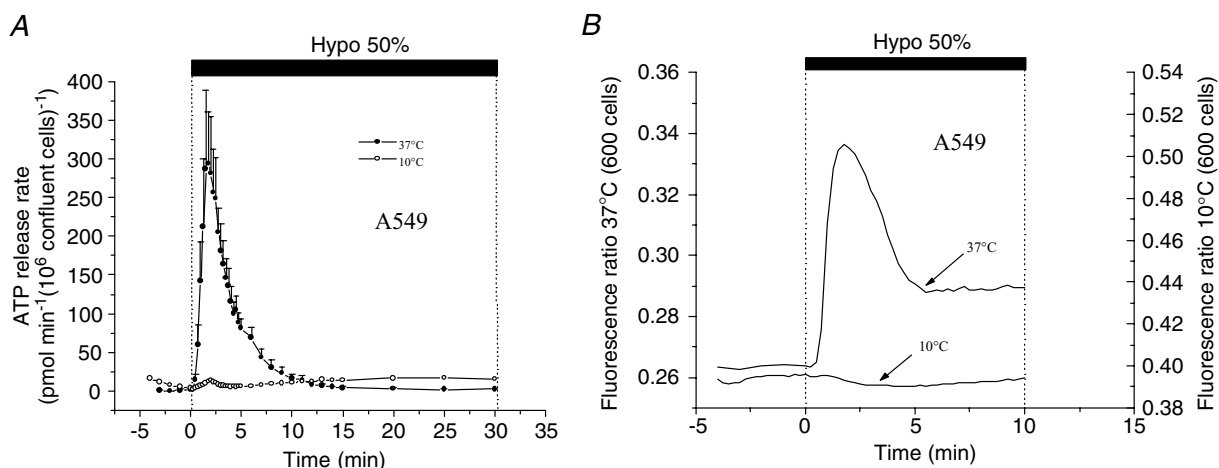


Figure 11. Hypotonic stress-induced ATP release is suppressed at low temperatures

A, release of ATP from A549 cells was almost completely abolished at 10°C ; the peak rate was $15 \text{ pmol min}^{-1} (10^6 \text{ confluent cells})^{-1}$, while cumulative release was $150 \text{ pmol} (10^6 \text{ confluent cells})^{-1}$. Perfusate temperature was reduced from 37°C to 10°C , 5 min prior to the experiment, and hypotonic stress-induced ATP release was measured as described in Methods (O). The trace showing ATP secretion from control cells (37°C , ●) is reproduced from Fig. 2. B, hypotonicity-induced $[\text{Ca}^{2+}]_i$ increase was inhibited at 10°C . Cells were perfused with cold solution as described in A and $[\text{Ca}^{2+}]_i$ was measured before and during 50% hypotonic shock. The trace showing $[\text{Ca}^{2+}]_i$ in control cells (37°C) is reproduced from Fig. 8. Note that lowering temperature efficiently impeded both $[\text{Ca}^{2+}]_i$ increase (B) and ATP release (A).

Another novel result of this study is that during hypotonic swelling cells exhibit a volume plateau that precedes the RVD (Fig. 3A). It demonstrates that before RVD mechanisms are fully activated, epithelial cells cannot resist osmotic forces and swell passively until equilibrium is reached, as dictated by the imposed osmotic gradient.

An additional important finding of our study relates to the role of ATP in volume restoration. In contrast to some previous reports, we found no evidence that purinergic receptor activation is needed to initiate or maintain the volume restoration process as suggested by others (Roman *et al.* 1999; Light *et al.* 1999; Darby *et al.* 2003). Because of continuous perfusion during ATP efflux assay, ATP concentration in the flow chamber (Fig. 1A) rarely exceeded 100 nM, and was many times lower during cell volume measurements in the side-view chamber (Boudreault & Grygorczyk, 2004) due to the smaller number of cells under investigation. Such low ATP concentrations should not activate purinergic receptors, since their EC_{50} , as measured by a rise in $[Ca^{2+}]_i$, IP_3 synthesis or modulation of short-circuit current, is in the micromolar range (Warburton *et al.* 1989; Peterson *et al.* 1997; Homolya *et al.* 1999). In spite of this, we routinely observed complete volume restoration of 16HBE14o⁻ and A549 cells.

Finally, it is noteworthy that the Ca^{2+} -dependent mechanism for vesicular ATP release hints of a somewhat different mode of signalling by extracellular ATP, which resembles signal transmission in the synaptic cleft more than the longer-range autocrine/paracrine communication. Indeed, essential features of neuronal acetylcholine- or ATP-mediated synaptic transmission (Evans *et al.* 1992) are now evident in epithelial cells: an apparent low-affinity binding receptors (see above), ecto-ATPases to rapidly terminate the signal (Communi *et al.* 1999; Lazarowski *et al.* 2000) and foremost, a Ca^{2+} -sensitive pool of ATP-filled vesicles. All this indicates that many non-neuronal cells are equipped to send and receive ATP-mediated signals within confined compartments, such as regions of close physical contact between neighbouring cells. Reports that an Arg-Gly-Asp-(RGD) sequence, found in the first putative extracellular loop of P2Y₂ receptors, binds to $\alpha_v\beta_3$ integrins (Erb *et al.* 2001) and that endogenous P2X receptors are restricted to areas of cell contact and colocalize with VE-cadherin in human endothelial cells (Glass *et al.* 2002) may support this hypothesis. Clearly, much remains to be studied to reassess the exact role of such ATP signalling.

In summary, based on the data presented, we propose that Ca^{2+} -dependent vesicular exocytosis is a major mechanism of cell swelling-induced ATP release. Further investigations are needed to clarify mechanisms and sources of intracellular Ca^{2+} elevations and to

dissect individual Ca^{2+} -dependent steps involved in such mechanosensitive ATP release.

References

- Abraham EH, Prat AG, Gerweck L, Seneveratne T, Arcenci RJ, Kramer R, Guidotti G & Cantiello HF (1993). The multidrug resistance (mdr1) gene product functions as an ATP channel. *Proc Natl Acad Sci U S A* **90**, 312–316.
- Bankston LA & Guidotti G (1996). Characterization of ATP transport into chromaffin granule ghosts. Synergy of ATP and serotonin accumulation in chromaffin granule ghosts. *J Biol Chem* **271**, 17132–17138.
- Bibby KJ & McCulloch CA (1994). Regulation of cell volume and $[Ca^{2+}]_i$ in attached human fibroblasts responding to anisosmotic buffers. *Am J Physiol* **266**, C1639–C1649.
- Birder LA, Barrick SR, Roppolo JR, Kanai AJ, De Groat WC, Kiss S & Buffington CA (2003). Feline interstitial cystitis results in mechanical hypersensitivity and altered ATP release from bladder urothelium. *Am J Physiol Renal Physiol* **285**, F423–F429.
- Blaug S, Rymer J, Jalickee S & Miller SS (2003). P2 purinoceptors regulate calcium-activated chloride and fluid transport in 31EG4 mammary epithelia. *Am J Physiol Cell Physiol* **284**, C897–C909.
- Bodas E, Aleu J, Pujol G, Martin-Satue M, Marsal J & Solsona C (2000). ATP crossing the cell plasma membrane generates an ionic current in *Xenopus* oocytes. *J Biol Chem* **275**, 20268–20273.
- Bodin P & Burnstock G (1998). Increased release of ATP from endothelial cells during acute inflammation. *Inflamm Res* **47**, 351–354.
- Bodin P & Burnstock G (2001). Evidence that release of adenosine triphosphate from endothelial cells during increased shear stress is vesicular. *J Cardiovasc Pharmacol* **38**, 900–908.
- Boudreault F & Grygorczyk R (2002). Cell swelling-induced ATP release and gadolinium-sensitive channels. *Am J Physiol Cell Physiol* **282**, C219–C226.
- Boudreault F & Grygorczyk R (2004). Evaluation of rapid volume changes of substrate-adherent cells by conventional microscopy 3D imaging. *J Microsc* **215**, 302–312.
- Brown CD & Dudley AJ (1996). Chloride channel blockers decrease intracellular pH in cultured renal epithelial LLC-PK1 cells. *Br J Pharmacol* **118**, 443–444.
- Burnstock G (1987). Local control of blood pressure by purines. *Blood Vessels* **24**, 156–160.
- Burnstock G, Campbell G, Satchell D & Smythe A (1970). Evidence that adenosine triphosphate or a related nucleotide is the transmitter substance released by non-adrenergic inhibitory nerves in the gut. *Br J Pharmacol* **40**, 668–688.
- Burnstock G, Dumsday B & Smythe A (1972). Atropine resistant excitation of the urinary bladder: the possibility of transmission via nerves releasing a purine nucleotide. *Br J Pharmacol* **44**, 451–461.
- Chen Y, Zhao YH & Wu R (2001). Differential regulation of airway mucin gene expression and mucin secretion by extracellular nucleotide triphosphates. *Am J Respir Cell Mol Biol* **25**, 409–417.

- Communi D, Paindavoine P, Place GA, Parmentier M & Boeynaems JM (1999). Expression of P2Y receptors in cell lines derived from the human lung. *Br J Pharmacol* **127**, 562–568.
- Cotrina ML, Lin JH, Alves-Rodrigues A, Liu S, Li J, Azmi-Ghadimi H, Kang J, Naus CC & Nedergaard M (1998). Connexins regulate calcium signaling by controlling ATP release. *Proc Natl Acad Sci U S A* **95**, 15735–15740.
- Cozens AL, Yezzi MJ, Kunzelmann K, Ohrui T, Chin L, Eng K, Finkbeiner WE, Widdicombe JH & Gruenert DC (1994). CFTR expression and chloride secretion in polarized immortal human bronchial epithelial cells. *Am J Respir Cell Mol Biol* **10**, 38–47.
- Darby M, Kuzmiski JB, Panenka W, Feighan D & MacVicar BA (2003). ATP released from astrocytes during swelling activates chloride channels. *J Neurophysiol* **89**, 1870–1877.
- Erb L, Liu J, Ockerhausen J, Kong Q, Garrad RC, Griffin K, Neal C, Krugh B, Santiago-Perez LI, Gonzalez FA, Gresham HD, Turner JT & Weisman GA (2001). An RGD sequence in the P2Y₂ receptor interacts with $\alpha_v\beta_3$ integrins and is required for G_o-mediated signal transduction. *J Cell Biol* **153**, 491–501.
- Evans RJ, Derkach V & Surprenant A (1992). ATP mediates fast synaptic transmission in mammalian neurons. *Nature* **357**, 503–505.
- Gatof D, Kilic G & Fitz JG (2004). Vesicular exocytosis contributes to volume-sensitive ATP release in biliary cells. *Am J Physiol Gastrointest Liver Physiol* **286**, G538–G546.
- Glass R, Loesch A, Bodin P & Burnstock G (2002). P2X₄ and P2X₆ receptors associate with VE-cadherin in human endothelial cells. *Cell Mol Life Sci* **59**, 870–881.
- Grierson JP & Meldolesi J (1995). Shear stress-induced [Ca²⁺]_i transients and oscillations in mouse fibroblasts are mediated by endogenously released ATP. *J Biol Chem* **270**, 4451–4456.
- Grygorczyk R & Hanrahan JW (1997). CFTR-independent ATP release from epithelial cells triggered by mechanical stimuli. *Am J Physiol* **272**, C1058–C1066.
- Hazama A, Hayashi S & Okada Y (1998). Cell surface measurements of ATP release from single pancreatic beta cells using a novel biosensor technique. *Pflugers Arch* **437**, 31–35.
- Hazama A, Shimizu T, Ando-Akatsuka Y, Hayashi S, Tanaka S, Maeno E & Okada Y (1999). Swelling-induced, CFTR-independent ATP release from a human epithelial cell line: lack of correlation with volume-sensitive Cl[−] channels. *J Gen Physiol* **114**, 525–533.
- Hisadome K, Koyama T, Kimura C, Droogmans G, Ito Y & Oike M (2002). Volume-regulated anion channels serve as an auto/paracrine nucleotide release pathway in aortic endothelial cells. *J Gen Physiol* **119**, 511–520.
- Homolya L, Watt WC, Lazarowski ER, Koller BH & Boucher RC (1999). Nucleotide-regulated calcium signaling in lung fibroblasts and epithelial cells from normal and P2Y₂ receptor (−/−) mice. *J Biol Chem* **274**, 26454–26460.
- Kato K, Evans AM & Kozlowski RZ (1999). Relaxation of endothelin-1-induced pulmonary arterial constriction by niflumic acid and NPPB: mechanism(s) independent of chloride channel block. *J Pharmacol Exp Ther* **288**, 1242–1250.
- Lazarowski ER, Boucher RC & Harden TK (2000). Constitutive release of ATP and evidence for major contribution of ecto-nucleotide pyrophosphatase and nucleoside diphosphokinase to extracellular nucleotide concentrations. *J Biol Chem* **275**, 31061–31068.
- Lazarowski ER, Homolya L, Boucher RC & Harden TK (1997). Direct demonstration of mechanically induced release of cellular UTP and its implication for uridine nucleotide receptor activation. *J Biol Chem* **272**, 24348–24354.
- Lazarowski ER, Tarran R, Grubb BR, Van Heusden CA, Okada S & Boucher RC (2004). Nucleotide release provides a mechanism for airway surface liquid homeostasis. *J Biol Chem* **279**, 36855–36864.
- Li C, Ramjeesingh M & Bear CE (1996). Purified cystic fibrosis transmembrane conductance regulator (CFTR) does not function as an ATP channel. *J Biol Chem* **271**, 11623–11626.
- Light DB, Capes TL, Gronau RT & Adler MR (1999). Extracellular ATP stimulates volume decrease in *Necturus* red blood cells. *Am J Physiol* **277**, C480–C491.
- Maroto R & Hamill OP (2001). Brefeldin A block of integrin-dependent mechanosensitive ATP release from *Xenopus* oocytes reveals a novel mechanism of mechanotransduction. *J Biol Chem* **276**, 23867–23872.
- Missiaen L, de Smedt H, Parys JB, Sienaert I, Vanlingen S, Droogmans G, Nilius B & Casteels R (1996). Hypotonically induced calcium release from intracellular calcium stores. *J Biol Chem* **271**, 4601–4604.
- Mitchell CH, Carre DA, McGlinn AM, Stone RA & Civan MM (1998). A release mechanism for stored ATP in ocular ciliary epithelial cells. *Proc Natl Acad Sci U S A* **95**, 7174–7178.
- Morse DM, Smullen JL & Davis CW (2001). Differential effects of UTP, ATP, and adenosine on ciliary activity of human nasal epithelial cells. *Am J Physiol Cell Physiol* **280**, C1485–C1497.
- Niggel J, Sigurdson W & Sachs F (2000). Mechanically induced calcium movements in astrocytes, bovine aortic endothelial cells and C6 glioma cells. *J Membr Biol* **174**, 121–134.
- Oliver AE, Baker GA, Fugate RD, Tablin F & Crowe JH (2000). Effects of temperature on calcium-sensitive fluorescent probes. *Biophys J* **78**, 2116–2126.
- Peterson WM, Meggyesy C, Yu K & Miller SS (1997). Extracellular ATP activates calcium signaling, ion, and fluid transport in retinal pigment epithelium. *J Neurosci* **17**, 2324–2337.
- Prat AG, Reisin IL, Ausiello DA & Cantiello HF (1996). Cellular ATP release by the cystic fibrosis transmembrane conductance regulator. *Am J Physiol* **270**, C538–C545.
- Raat NJ, De Smet P, van Driessche W, Bindels RJ & Van Os CH (1996). Measuring volume perturbation of proximal tubular cells in primary culture with three different techniques. *Am J Physiol* **271**, C235–C241.
- Reddy MM, Quinton PM, Haws C, Wine JJ, Grygorczyk R, Tabcharani JA, Hanrahan JW, Gunderson KL & Kopito RR (1996). Failure of the cystic fibrosis transmembrane conductance regulator to conduct ATP. *Science* **271**, 1876–1879.
- Roman RM, Feranchak AP, Davison AK, Schwiebert EM & Fitz JG (1999). Evidence for Gd³⁺ inhibition of membrane ATP permeability and purinergic signaling. *Am J Physiol* **277**, G1222–G1230.

- Sabirov RZ, Dutta AK & Okada Y (2001). Volume-dependent ATP-conductive large-conductance anion channel as a pathway for swelling-induced ATP release. *J Gen Physiol* **118**, 251–266.
- Sauer H, Hescheler J & Wartenberg M (2000). Mechanical strain-induced Ca^{2+} waves are propagated via ATP release and purinergic receptor activation. *Am J Physiol Cell Physiol* **279**, C295–C307.
- Stout CE, Costantin JL, Naus CC & Charles AC (2002). Intercellular calcium signaling in astrocytes via ATP release through connexin hemichannels. *J Biol Chem* **277**, 10482–10488.
- Taylor AL, Kudlow BA, Marrs KL, Gruenert DC, Guggino WB & Schwiebert EM (1998). Bioluminescence detection of ATP release mechanisms in epithelia. *Am J Physiol* **275**, C1391–C1406.
- Unsworth CD & Johnson RG (1990). Acetylcholine and ATP are coreleased from the electromotor nerve terminals of *Narcine brasiliensis* by an exocytotic mechanism. *Proc Natl Acad Sci U S A* **87**, 553–557.
- Warburton D, Buckley S & Cosico L (1989). P1 and P2 purinergic receptor signal transduction in rat type II pneumocytes. *J Appl Physiol* **66**, 901–905.
- Zhang Y & Hamill OP (2000). On the discrepancy between whole-cell and membrane patch mechanosensitivity in *Xenopus* oocytes. *J Physiol* **523**, 101–115.

Acknowledgements

This study was supported in part by the Canadian Institutes of Health Research, the Canadian Cystic Fibrosis Foundation (CCFF) and the Canadian Foundation for Innovation. F.B. was the recipient of a CCFF studentship. The authors thank Dr Yves Berthiaume for his comments on the manuscript, Nicolas Groulx for his assistance in some ATP efflux experiments, and Ovid M. Da Silva, Editor, Research Support Office, Research Centre, CHUM, for editing this text.